

Analytical Modeling of Characteristic Maps of the SR-30 Turbojet Engine

Joaquín Valencia Bravo*, Frederick Just Agosto,
David Serrano Acevedo, Marco Menegozzo
Department of Mechanical Engineering
University of Puerto Rico -Mayagüez
Mayagüez, Puerto Rico

Orlando Ruiz Quinones
Writing Systems Engineer, Hewlett Packard Inc.
Aguadilla, Puerto Rico

Abstract—A crucial step in the mathematical modeling of a gas turbine engine is the characteristic map development of its main components, the compressor and the turbine. Maps can be obtained from manufacturers, although they are generally not available to the user. Furthermore, the construction of these maps through experiments is expensive. Analytical models prove to be economically more advantageous. Compared to other methods, they require little experimental data to be validated. These models are based on physical principles, so the results are more accurate compared to those obtained through numerical simulations or the use of neural networks. This approach allows more flexibility to make changes to the performance characteristics of engine components. These changes may be achieved by modifying certain geometric measurements, this quality could be used in diagnostic and/or engine control systems. In this work the characteristic map of the SR-30 turbojet engine components is analytically modeled. Geometric dimensions and properties of the working fluid were taken as data. This is an one-dimensional model in which it is analyzed the aerodynamics and thermodynamics parameters in each station of the centrifugal compressor and axial turbine. Design point calculations are used to estimate the values of working fluid parameters such as velocity, pressure, temperature, enthalpy, and entropy function. Results of this work are compared with those obtained by other authors. For greater reliability in these results, an experimental validation is necessary.

Keywords — Turbojet engine; characteristic map; analytical model; compressor; turbine

I. INTRODUCTION

Turbomachinery component performance maps constitute an essential input to the development of engine performance models. Maps may be obtained from experimental procedures, but this can result in an expensive endeavor. Furthermore, experiments might not completely describe the full range of interest, and the use of extrapolation is required. Manufacturers usually develop product component characteristic maps but this information is rarely distributed to customers. In addition to experimental methods, there are other alternatives in

obtaining performance maps. Kurzke [1] used data from published maps to reproduce component maps through commercial programs such as Smooth_C [2] and Smooth_T [3]. Lazzaretto et al. [4] developed artificial machine maps using generalized maps taken from literature with appropriate scaling techniques. Results were validated with test measurements from real plants. Many authors have used neural networks approaches. Gustafson et al. [5] obtained steady-state compressor performance maps from correlations of transient compressor maps. The learned correlations were expected to provide information for predicting stall and surge inception. Yu et al. [6] predicted an axial compressor's performance map based on neural networks. Training was performed with experimental results provided from manufacturers. Ghorbanian et al. [7] used different types of neural networks to simulate the performance maps of an axial compressor; data was obtained from a compressor rig test. Jiang et al. [8] developed an analytical model for the centrifugal compressor based on first principles where energy transfer is taken into consideration. The dynamic performance including losses was determined from the compressor geometry. In addition incident and friction losses were modeled while the clearance, backward and volute losses were considered constants for all off-design conditions. Witkowski et al. [9] developed a one-dimensional analysis for the SR-30 gas turbine components used in education and research settings. Based on design point performance, the flow through the radial compressor and the one stage axial turbine was computed. The corresponding initial conditions of the flow along with the dimensions for each component were used. Losses were estimated using Stodola's equation for slip factor calculations. These calculations were only presented for a design speed of 78000 rpm. Studies in developing the component maps of a SR-30 turbine were performed by various authors taking into consideration the design point analysis developed by Witkowski et al. [9]. May et al. [11] described a procedure to obtain the velocity triangles for the characteristic maps of the SR-30 gas turbine. An

iterative calculation in Excel was used, but the mathematical analysis to achieve this goal was not presented. Resulting maps were plotted using the Smooth-C and Smooth-T commercial softwares. The model has been used to monitor health operation of the engine. Based on the mean-line analysis, Léonard et al. [10] developed the compressor characteristic curves. The results were stored in a line format to prevent numerical interpolation problems. These authors did not use a map for the turbine, instead, it was characterized using Stodola's ellipsis equations. Compressor and turbine losses were considered in the calculation of the velocity triangles. Oh et al. [11] tested most of the loss models previously published in the literature. They found an optimum set of empirical loss models for a reliable performance prediction of centrifugal compressors. May et al. [12] cites these loss correlations for the calculation of the compressor map. In radial flow machines, like centrifugal compressors, the angular momentum imparted to the flow is reduced by a factor known as the slip factor. von Backström [13] developed a method that unifies the trusted centrifugal impeller slip factor prediction methods of Busemann [14], Stodola [15], Stanitz [16], Wiesner [20], Eck [17] and Csanady (reported by Dixon [18]) in one equation. This equation, which is used in the present work, may be adjusted for specifically constructed families to improve the accuracy of the prediction. There is no compressor map or turbine map available for the SR-30 turbojet engine that has been validated using experimental data.

The present work develops an analytical model of the SR-30's component maps. A one-dimensional approach is applied to perform the calculation at the design point performance. The final goal is to produce tabulated functions that may be introduced into an engine model. In addition, interpolation will be applied to obtain values of the dependent parameters such as the referred mass flow rate \dot{m} , the pressure ratio PR and the efficiency η .

II. ANALYTICAL MODEL

In this section, the analytical model of the component maps is described. The design point and off design performance are conducted taking into account the limits of the engine operation. Design point calculations are based on iterative procedures. This consist on assuming a value of the axial velocity component, then, performing the calculations required to find the aero-thermodynamic properties of the fluid and finally recalculating the assumed velocity. Iteration is finished when the difference between the initial guess and the calculated axial flow velocity is within the imposed tolerance. As a result, the value obtained for the remaining fluid parameters will be found. Compressor map and turbine map models are described separately. The properties of the working fluid in a gas turbine engine have a powerful impact upon its performance. The working fluid, which passes through the compressor, is assumed as dry air and the working fluid that passes through the turbine is assumed as the product of combustion; the mixture of dry air and kerosene fuel. Water content due to humidity is neglected. The correlations used for the fluid properties were taken from Walsh et al. [19]. The equations

required to find the energy losses in the centrifugal compressor was obtained from Oh et al. [11], and the loss coefficients in the turbine, were taken from Dixon [18] and Cohen et al. [20]. Moreover, the thermodynamic relations used are derived from the Mollier diagram found in Dixon [18].

A. Compressor Map

The SR-30 turbojet engine uses a centrifugal compressor. The analysis for the flow through the compressor is based in the one-dimensional steady flow analysis, in which according to Dixon [18], the velocity and density are regarded as uniform across each section of a duct or passage. By continuity, the mass flow rate (\dot{m}) through the compressor is given by

$$\dot{m} = \rho_1 C_{a1} A_1 = \rho_{2I} C_{a2I} A_{2I} = \rho_{2D} C_{a2D} A_{2D} = \rho_2 C_{a2} A_2 \quad (1)$$

In equation (1), ρ , C_a and A denote the air density, air axial velocity and the cross-sectional area respectively. The subscripts 1, 2I, 2D and 2 denote stations corresponding to the entrance to impeller, exit from impeller, entrance to vaned diffuser and the exit from vaned diffuser, respectively. These stations can be visualized in Fig. 1.

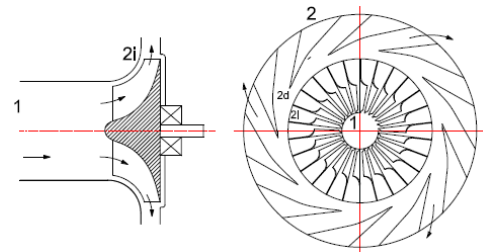


Figure 1. Nomenclature of stations used in the compressor

Compressor maps will be developed from data points obtained from calculations of the performance parameters such as: mass flow rate \dot{m} , rotational speed N , pressure ratio PR_c and isentropic efficiency η_c . For this purpose, velocity triangles are calculated initially at the design point. At this point, the mass flow rate and the rotational speed are $\dot{m} = 0.297 \text{ kg/s}$ and $N = 78000 \text{ rpm}$, respectively. In addition, the geometric data and input conditions published by Witkowski et al. [9] are used.

The first velocity triangle, depicted in Fig.2, is calculated at the impeller inlet. According to this triangle, the relation between the velocity vectors is given by

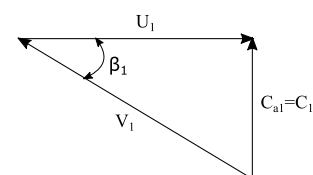


Figure 2. Velocity triangle at impeller inlet

$$V_1 = C_1 - U_1 \quad (2)$$

where V_1 and C_1 are the relative and absolute velocity of the air, respectively. The term U_1 denotes the impeller eye velocity vector or tangential velocity vector. It is assumed that the air enters the impeller eye in the axial direction, i.e., $C_1 = C_{a1}$. The angle between the relative velocity and the tangential velocity is $\beta_1=57^\circ$. At the impeller inlet (known also as eye or inducer), the effective diameter is defined according to

$$D_1 = \sqrt{0.5(D_t^2 + D_r^2)} \quad (3)$$

where D_t is the diameter at the impeller eye tip and D_r is the diameter at the impeller eye root. The annulus area of impeller eye is

$$A_1 = \frac{\pi}{4}(D_t^2 - D_r^2) \quad (4)$$

The mean tangential speed at the inducer may be calculated by

$$U_1 = \pi D_1 N \quad (5)$$

In addition, velocities at impeller eye tip ($U_t = \pi D_t N$) and at impeller eye root ($U_r = \pi D_r N$) may be found. It is important to check that the velocities at the impeller eye tip should be less than the speed of sound ($M_t < 1$) to avoid breakdown of flow and excessive pressure loss. To calculate the axial component of the absolute velocity C_{a1} , a trial and error process will be performed. Fig.3 shows the iterative procedure followed to obtain the parameters at compressor inlet or station 1, according to this flow diagram, the density is calculated on the basis of the known stagnation temperature and pressure. From the continuity equation an initial estimate of the axial velocity C_{a1} is obtained. With this value and with the help of thermodynamic relations from the Mollier diagram, the density is recalculated, and the actual velocity is determined from the continuity equation. If the assumed and calculated velocities do not coincide, it is necessary to iterate until convergence is reached.

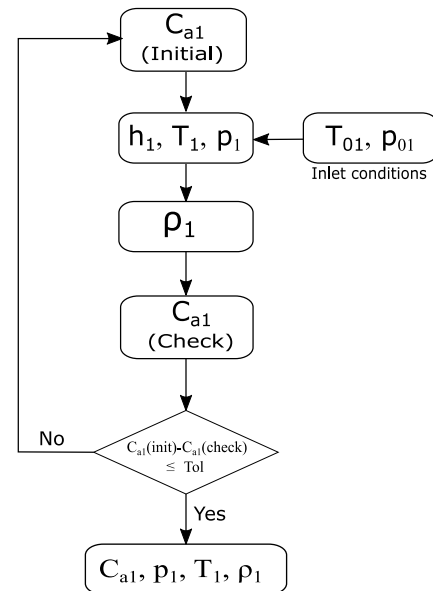


Figure 3. Flow diagram of the iterative procedure at the impeller inlet

Equations required to calculate C_{a1} , are presented. The static enthalpy h_1 may be obtained by

$$h_1 = h_{01} - \frac{1}{2} C_1^2 \quad (6)$$

where h_{01} is obtained from a polynomial function dependent on the temperature T_{01} , i.e. $h_{01} = f_h(T_{01})$. The static pressure p_1 is given by

$$p_1 = \frac{p_{01}}{e^{\frac{\phi_{01} - \phi_1}{R}}} \quad (7)$$

Here, p_{01} is the total pressure. The terms ϕ_{01} and ϕ_1 are functions dependent on the temperature T_{01} and T_1 , i.e. $\phi_{01} = f_\phi(T_{01})$ and $\phi_1 = f_\phi(T_1)$. The air density may be calculated from the equation of state for a perfect gas, thus

$$\rho_1 = \frac{p_1}{RT_1} \quad (8)$$

where R is the gas constant for the air and T_1 may be found as a function of the enthalpy h_1 , i.e. $T_1 = f_h(h_1)$. Finally, the axial velocity C_{a1} is given by

$$C_{a1} = \frac{\dot{m}}{\rho_1 A_1} \quad (9)$$

Additional calculations are considered to obtain the relative velocity V_1 , $V_1 = \sqrt{C_1^2 - U_1^2}$ and the absolute Mach number, $M_{1abs} = C_1 / \sqrt{\gamma RT}$.

The velocity triangle at the impeller tip is shown in Fig.4.

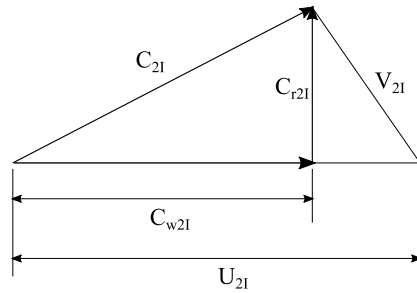


Figure 4. Velocity triangle at impeller outlet

According to Fig. 4, the air leaves the impeller tip with an absolute velocity C_{2I} . This velocity has a tangential or whirl component C_{w2I} and a small radial component C_{r2I} , they are related by

$$C_{2I} = \sqrt{C_{w2I}^2 + C_{r2I}^2} \quad (10)$$

Under ideal conditions the whirl component will be equal to the impeller tip speed U_{2I} . Due to the relative eddies in the impeller blade passage the impeller exit flow angle differs from the impeller exit blade angle; a measure of deviation can be calculated using the concept of a slip factor. There are many correlations predicting the slip factor. Von Backström [13] describes a method that unifies the centrifugal impeller slip factor (σ). The prediction method of Dixon [18]), that uses one equation, will be used. This equation is given by

$$\sigma = 1 - \frac{1}{1 + F_o \left(\frac{1}{S_e} \right) (\cos \beta)^{0.5}} \quad (11)$$

where F_o is a correction constant corresponding to the compressor. This value is adjusted to improve the accuracy of the prediction. The blade angle at impeller exit is denoted by β . The ratio given l/S_e is known as the blade row solidity. The blade length l and blade spacing S_e are determined with $l = (r_e - r_i) / \cos \beta$ and $S_e = 2\pi r_e / n_b$. The terms r_i and r_e are the radius of the blade leading edge and blade trailing edge, respectively and the number of blades is denoted by n_b . The area at impeller exit, A_{2I} , and the blade speed U_{2I} are calculated with $A_{2I} = \pi D_{2I} b_{2I}$ and $U_{2I} = \pi D_{2I} N$ respectively. The terms D_{2I} and b_{2I} are the impeller tip diameter and the axial width at impeller exit respectively. In terms of the slip factor and the blade tangential speed, the whirl component of the absolute velocity C_{w2I} are determined with

$$C_{w2I} = \sigma U_{2I} \quad (12)$$

Some designers consider the value of the radial component C_{rI} the same as the inlet axial velocity C_{aI} (Cohen et al.[20]), but, in the current model it is obtained with an estimated value based on equation (10). The final value of the radial component is determined following an iteration procedure which is shown in Figure 5.

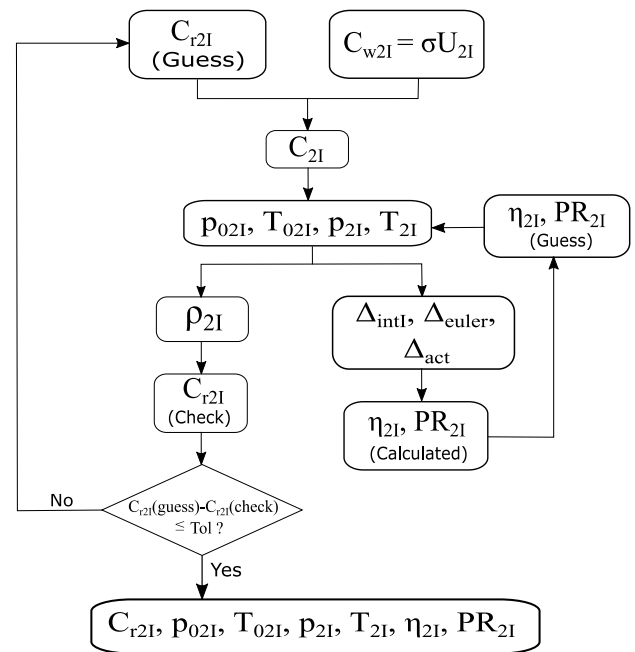


Figure 5. Flow diagram of the iterative procedure at the impeller outlet

According to the diagram shown in Fig. 5, static and stagnation pressures and temperatures have to be determined. Thus, the total pressure p_{02I} is given by

$$p_{02I} = p_{0I} PR_{2I} \quad (13)$$

In equation (13), p_{0I} is given as data and PR_{2I} is the pressure ratio. Initially PR_{2I} is guessed and then calculated. The stagnation temperature T_{02I} may be obtained from a correlation function of the stagnation enthalpy h_{02I} , i.e. $T_{02I} = f_T(h_{02I})$. The enthalpy h_{02I} is given by

$$h_{02I} = h_{0I} + \frac{h_{02Is} - h_{0I}}{\eta_{2I}} \quad (14)$$

where h_{0I} may be obtained from a correlation in function of the stagnation temperature T_{0I} which is given as data. The term η_{2I} denotes the efficiency that is initially guessed and finally calculated after some iterations. The stagnation enthalpy at an isentropic process h_{02Is} is obtained by the correlation function $h_{02Is} = f_h(T_{02Is})$. In the same way, the temperature T_{02Is} may be given by the correlation function $T_{02Is} = f_T(\phi_{02Is})$. The term ϕ_{02Is} is an entropy function obtained by the following expression

$$\phi_{02Is} = \phi_{0I} + R \ln \left(\frac{p_{02I}}{p_{0I}} \right) \quad (15)$$

where the entropy function ϕ_{0I} is obtained using the correlation function $\phi_{0I} = f_\phi(T_{0I})$. The static temperature T_{2I} is given in terms of the static enthalpy h_{2I} with the

correlation function $T_{2I} = f_T(h_{2I})$. The enthalpy h_{2I} is calculated with the expression

$$h_{2I} = h_{02I} - \frac{1}{2} C_{2I}^2 \quad (16)$$

The static pressure p_{2I} is given by

$$p_{2I} = \frac{p_{02I}}{e^{\frac{\phi_{02I} - \phi_{2I}}{R}}} \quad (17)$$

here the entropy functions ϕ_{02I} and ϕ_{2I} are given in term of the temperatures T_{02I} and T_{2I} respectively, i.e. $\phi_{02I} = f_\phi(T_{02I})$ and $\phi_{2I} = f_\phi(T_{2I})$. The density and the radial component of absolute velocity are calculated using $\rho_{2I} = p_{2I}/(RT_{2I})$ and $C_{r2I} = \dot{m}/(\rho_{2I}A_{2I})$ respectively. The Mach numbers should be calculated to ensure that the flow does not exceed the velocity of sound. The performance parameters are also affected by losses that occur inside the compressor. The correlations used for the compressor losses were taken from Oh et al. [22] and Jiang et al. [8]. The pressure ratio and isentropic efficiency may be given by

$$PR_{2I} = \left[\left(\frac{\Delta h_{euler} - \sum \Delta h_{int}}{c_p T_{01}} \right) + 1 \right]^{\gamma/(\gamma-1)} \quad (18)$$

and

$$\eta_{2I} = \frac{\Delta h_{euler} - \sum \Delta h_{int}}{\Delta h_{act}} \quad (19)$$

where, Δh_{euler} is the ideal specific enthalpy change of the working fluid which depends on the slip factor and the tangential velocity of the blades at the impeller tip. Thus $\Delta h_{euler} = \sigma U_{2I}^2$. The term $\sum \Delta h_{int}$ represents the summation of all internal losses in the impeller such as incidence loss, blade loading loss, skin friction loss and clearance loss, thus $\sum \Delta h_{int} = \Delta h_i + \Delta h_{bld} + \Delta h_{sf} + \Delta h_{cl}$. The actual specific enthalpy denoted by Δh_{act} , is the sum of the ideal specific enthalpy change and the parasitic loss correlations ($\Delta h_{act} = \Delta h_{euler} + \sum \Delta h_{prs}$). The parasitic losses, $\sum \Delta h_{prs}$, are assumed to be the sum of the disc friction loss, recirculation loss and the leakage loss, i.e. $\sum \Delta h_{prs} = \Delta h_{df} + \Delta h_{rc} + \Delta h_{lk}$.

The velocity triangle at the vaned diffuser inlet is depicted in Fig. 6.

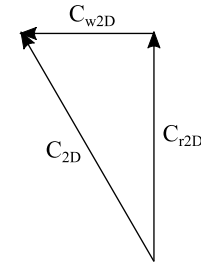


Figure 6. Velocity triangle at the vaned diffuser inlet

In Fig. 6, only the absolute velocity C_{2D} and its components are present. The relative velocity vanishes because there is no moving element. To determine the whirl component C_{w2D} of C_{2D} , the conservation of the angular momentum within the vaneless diffuser can be assumed, i.e. $C_{w2D} r_{2D} = C_{w2I} r_{2I}$. Thus, the whirl component of the velocity is given by

$$C_{w2D} = \frac{C_{w2I} r_{2I}}{r_{2D}} \quad (20)$$

The area and absolute velocity are obtained from $A_{2D} = 2\pi r_{2D} b_{2D}$ and $C_{2D} = \sqrt{C_{r2D}^2 + C_{w2D}^2}$ respectively. The iterative procedure performed here is similar to that followed at the impeller exit. No further energy is supplied to the air after it leaves the impeller, so that neglecting the effect of friction, the angular momentum must be constant (Cohen et al. [20]). The above implies that no work is done in the vaneless diffuser and the process is adiabatic. Thus, the following relation is obtained

$$h_{02I} = h_{02D} \quad (21)$$

The pressure ratio and isentropic efficiency is calculated in the same way as in the last stage. Although here, Δh_{intI} is substituted by Δh_{intVD} which correspond to the losses in the impeller and the vaneless diffuser, as follows: $\Delta h_{intVD} = \Delta h_{intI} + \Delta h_{vld}$.

Finally, calculations of the velocity triangle at the diffuser output are performed. Here, the whirl component of the velocity, is found using conservation of angular momentum, which yields $C_{w2} = C_{w2D} r_{2D}/r_2$. The area and the absolute velocity (magnitude) are $A_2 = 2\pi r_2 b_2$ and $C_2 = \sqrt{C_{a2}^2 + C_{w2}^2}$ respectively. The iterative procedure to obtain the velocities and the thermodynamic states are similar to the previous stations. Assumptions done for the station of vaneless diffuser may be applied for the vaned diffuser, thus $h_{02D} = h_{02}$. In the calculations of the pressure ratio and the isentropic efficiency, the losses through the entire compressor stage (i.e., impeller, vaneless diffuser and vaned diffuser) have to be considered. These losses denoted by Δh_{intT} may be obtained by $\Delta h_{intT} = \Delta h_{intVD} + \Delta h_{iD} + \Delta h_{sfD}$, where Δh_{intVD} represents the internal losses in the impeller and vaneless diffuser, Δh_{iD} is the incidence loss in the diffuser, and Δh_{sfD} is the skin friction loss in the diffuser.

The velocity triangles corresponding to the off-design performance are constructed taking into account the mass

flow rate and rotational speed in the range of $\dot{m} = 0 - 0.5 \text{ kg/s}$ and $N = 50000 - 90000 \text{ rpm}$, respectively. In the off-design calculations it is assumed that the absolute inlet velocity remains axial and the design point value of the slip factor was constant for all off-design conditions.

B. Turbine Map

The SR-30 is a single stage axial turbine composed of one row of nozzles and one rotor. Figure 7 shows the nomenclature of the stages employed in the calculations; N refers to the nozzle and R the rotor.

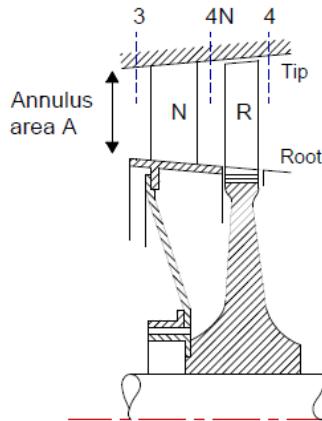


Figure 7. Nomenclature of stations used for the turbine

Ainley and Mathieson correlations [18] were used to calculate the energy losses. These estimated losses will be useful in obtaining characteristic parameters such as the mass flow rate \dot{m} , the rotational speed N , the pressure ratio PR_t and the efficiency η . The operating conditions used in establishing the design point velocity triangles were: $\dot{m} = 0.3 \text{ kg/s}$ and $N = 78000 \text{ rpm}$. A mean annulus diameter is assumed in the calculations. This approach is valid when the ratio of the tip radius r_t to the root radius r_r is low ($r_t/r_r = 1:38$). The turbine considered in this work meets this low aspect ratio. Moreover, we can consider the mean diameter equal in all stations because the difference between the station mean diameters are negligible. Thus, the effective mean diameter may be given by $D_m = \sqrt{0.5(D_r^2 + D_t^2)}$. With the effective diameter and the rotational speed, the mean blade speed is $U = \pi D_m N$. The mean annulus area is calculated by $A_m = \pi(D_r^2 - D_t^2)/4$.

Geometric dimensions and inlet conditions were extracted from Witkowski et al. [9]. By using the geometric measurements of the turbine, a tip clearance of 0.54 mm was obtained. It is assumed that the stator blades have the same shape as the rotor blades. The fluid through the turbine is the air-fuel combustion products.

Fig. 8 depicts the velocity configurations at each station in this turbine. In a single-stage turbine the velocity at turbine inlet C_3 will be axial (Cohen et al. [20]), thus, $C_3 = C_{a3}$ (C_{a3} is the axial component of the velocity at turbine inlet or station 3). The value of this velocity will be taken as constant for all off-design conditions.

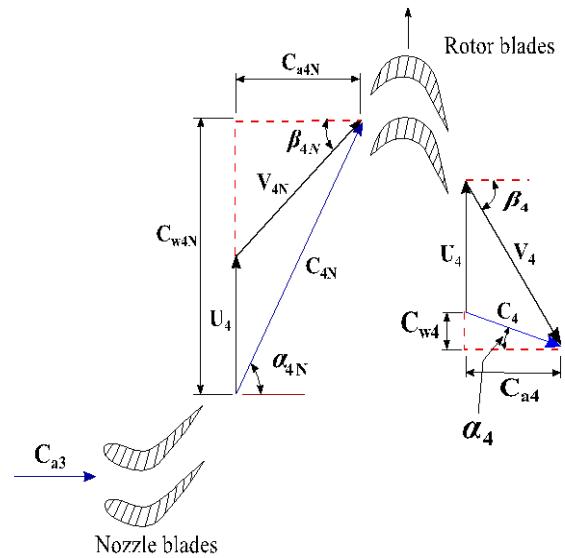


Figure 8. Velocity diagram of the axial turbine stage

Fig.9 shows the iterative procedure to calculate C_{a3} . This procedure is similar to the calculations made at compressor inlet.

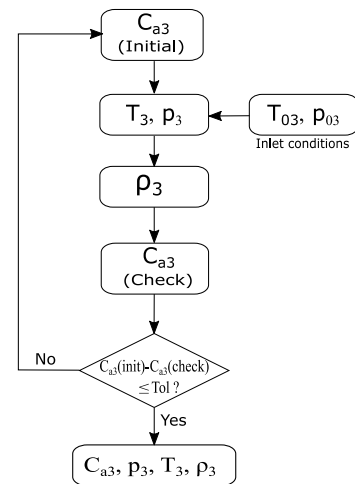


Figure 9. Flow diagram of the iterative procedure at the nozzle inlet

Initially, the velocity C_{a3} is guessed. Then, the static temperature is found using a correlation in terms of the static enthalpy h_3 , i.e. $T_3 = f_T(h_3)$. The enthalpy h_3 is obtained by

$$h_3 = h_{03} - \frac{1}{2} C_3^2 \quad (22)$$

where: $h_{03} = f_h(T_{03}, FAR)$ and FAR is the fuel-air ratio. The static pressure is obtained using

$$p_3 = \frac{p_{03}}{e^{\frac{\phi_{03} - \phi_3}{R}}} \quad (23)$$

where $\phi_{03} = f_\phi(T_{03})$ and $\phi_3 = f_\phi(T_3)$. Similarly to previous cases, the density is calculated with $\rho_3 = p_3 / (RT_3)$. From the continuity equation, the axial velocity C_{a3} is calculated by $C_{a3} = \dot{m} / (\rho_3 A_m)$. Finally, the corresponding mach number is determined using $M_{3abs} = C_3 / \sqrt{\gamma RT_3}$.

Fig. 8 shows the velocity triangle at the nozzle outlet or station 4N. It is assumed that the nozzle angle (α_{4N}) and the angular momentum at outlet remains constant. Therefore, for all off-design conditions the deviation of flow across the nozzle remains constant, thus $\alpha_{4N} = \text{constant}$. As a result, the relationship between the whirl component C_{w4N} and the axial component C_{a4N} (notation shown in Fig.8) will be constant according to the relation.

$$\alpha_{4N} = \tan^{-1} \left(\frac{C_{w4N}}{C_{a4N}} \right) \quad (24)$$

Since no work is done (adiabatic process) by the gas in the nozzle, the stagnation enthalpy must be constant over the annulus at the outlet. Thus, $h_{04N} = h_{03}$. Fig.10 shows the flow chart used for the iterative procedure to obtain the axial component of the absolute velocity C_{a4N} .

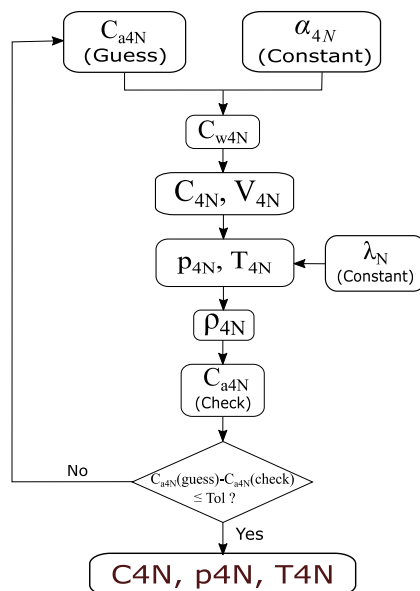


Figure 10. Flow diagram of the iterative procedure at the nozzle outlet

According to this flowchart, the absolute velocity C_{a4N} is guessed. Using this value and the angle α_{4N} , the velocity component C_{w4N} is obtained ($C_{w4N} = C_{a4N} \tan \alpha_{4N}$). The absolute velocity C_{4N} is given by $C_{4N} = \sqrt{C_{a4N}^2 + C_{w4N}^2}$. The static temperature T_{4N} is found in term of the enthalpy, i.e. $T_{4N} = f_T(h_{4N})$. The static enthalpy h_{4N} is given by

$$h_{4N} = h_{04N} - \frac{1}{2} C_{4N}^2 \quad (25)$$

The static pressure may be calculated by

$$p_{4N} = \frac{p_{03}}{e^{\frac{\phi_{03} - \phi_{4N}}{R}}} \quad (26)$$

Where, $\phi_{03} = f_\phi(T_{03}, FAR)$, $\phi_{4Ns} = f_\phi(T_{4Ns}, FAR)$, and $T_{4Ns} = f_T(h_{4Ns}, FAR)$. The enthalpy under isentropic process h_{4Ns} is found using

$$h_{4Ns} = h_{4N} - \lambda_N \frac{C_{4N}^2}{2} \quad (27)$$

where the total loss coefficient in the nozzle is denoted by λ_N . Neglecting the effect of friction, the critical pressure ratio is

$$\frac{p_{03}}{p_c} = \left(\frac{\gamma + 1}{2} \right)^{\frac{\gamma}{\gamma - 1}} \quad (28)$$

If $P_{03}/P_{4N} < P_{03}/P_c$, then the nozzle is not choked, otherwise, it is choked. The density ρ_{4N} and the axial flow velocity C_{a4N} are as follow $\rho_{4N} = p_{4N} / (RT_{4N})$ and $C_{a4N} = \dot{m} / (\rho_{4N} A_m)$. The absolute velocity and relative flow angle are $V_{4N} = \sqrt{(C_{w4N} - U_4)^2 + C_{a4N}^2}$ and $\beta_{4N} = \tan^{-1} [(C_{w4N} - U_4) / C_{a4N}]$.

The velocity triangle at rotor outlet or station 4 is depicted in Fig. 8. The flow diagram of the iterative procedure at this station is presented in Fig. 11.

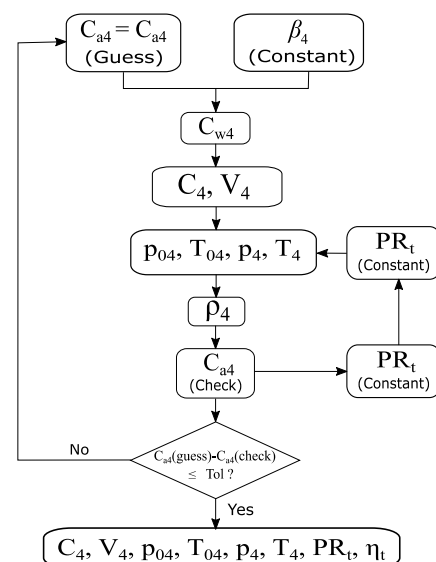


Figure 11. Flow diagram of the iterative procedure at the rotor outlet

According to this diagram, the exit angle β_4 is constant and it is calculated from the equations recommended by Ainley and Mathieson (Dixon [18]), thus

$$\beta_4 = -11.5 + 1.154 \cos^{-1} \left(\frac{\theta}{s} \right) + \frac{4s}{e} \quad (29)$$

In equation (29), θ is the throat width, s is the pitch and e is the mean radius of curvature of the blade suction surface. Equation (29) is for low outlet Mach numbers, i.e. $0 < M_4 < 0.5$. If $M_4 \geq 1$ the angle β_4 is calculated using $\beta_4 = \cos^{-1}(\theta/s)$. More details about this angle can be found in Dixon [18]. Initially, the axial component of the absolute velocity C_{a4} is guessed using the equality $C_{a4} = C_{a4N}$. The whirl component of the absolute velocity C_{w4} may be evaluated by

$$C_{w4} = C_{a4} \tan \beta_4 - U_4 \quad (30)$$

The absolute and relative velocity can be found similarly as in the other stations. The static temperature is found by the correlation $T_4 = f_T(h_4, FAR)$. The static enthalpy h_4 is given by

$$h_4 = h_{04} - \frac{C_4^2}{2} \quad (31)$$

where h_{04} is calculated by

$$h_{04} = h_{03} - UC_{a4N} \left(\frac{2U}{C_{a4N}} + \tan \beta_{4N} - \frac{C_{a4}}{C_{a4N}} \tan \beta_4 \right) \quad (32)$$

In equation (32), the stagnation enthalpy h_{03} is obtained by $h_{03} = f_h(T_{03}, FAR)$. Using the stagnation enthalpy h_{04} , the stagnation temperature is computed with $T_{04} = f_T(T_{03}, FAR)$. The stagnation pressure is found from

$$P_{04} = \frac{P_{03}}{PR_t} \quad (33)$$

where PR_t is the total pressure ratio which is guessed initially and then calculated by $PR_t = (\phi_{03} - \phi_{04ss})/R$. The entropy function ϕ_{03} is obtained using $\phi_{03} = f_\phi(T_{03}, FAR)$.

The stagnation entropy function ϕ_{04ss} is given by $\phi_{04ss} = \phi_{4ss} + R \ln(p_{04}/p_4)$. The static entropy function ϕ_{4ss} is obtained from the correlation $\phi_{4ss} = f_\phi(T_{4ss}, FAR)$

where the static temperature T_{4ss} is calculated using the correlation $T_{4ss} = f_T(h_{4ss}, FAR)$. The static enthalpy h_{4ss} is given by $h_{4ss} = h_{4s} - (T_4/T_{4N})(h_{4N} - h_{4Ns})$. The static isentropic enthalpy h_{4s} is found using

$$h_{4s} = h_4 - \lambda_R \frac{V_4^2}{2} \quad (34)$$

where λ_R is the total loss coefficient in the turbine rotor. The static pressure p_4 was calculated with

$$p_4 = \frac{P_{04}}{e^{\frac{\phi_{04} - \phi_4}{R}}} \quad (35)$$

here $\phi_{04} = f_\phi(T_{04}, FAR)$ and $\phi_4 = f_\phi(T_4, FAR)$. The isentropic efficiency is determined using

$$\eta_t = \frac{h_{03} - h_{04}}{h_{03} - h_{04ss}} \quad (36)$$

The density and the axial velocity component are calculated using equations similar to the previous cases. In addition, the mach number M_4 may be found by $M_4 = V_4 / \sqrt{\gamma RT_4}$. After doing the design point performance analysis, the off-design performance is obtained varying the speed and the mass flow rate. The speed was varied from 50000rpm to 90000rpm and the mass flow rate was varied until the design value was reached (0.3kg/s). The deviation of flow across the nozzle is assumed as constant at all off-design conditions. Because α_{4N} is constant the losses across the nozzle remain constant for all off-design conditions.

III. RESULTS

A. Compressor Map

Results of pressure, temperature, absolute velocity and Mach number in the behavior of the design point are shown in Table I. The values presented here correspond to each station in the compressor. The analysis was generated under the rotational speed of 78000rpm with a mass flow rate of 0.297kg/s. The abbreviation, PW, means present work. The table shows that the highest stagnation pressure is reached at the impeller outlet ($P_0 = 323kPa$). The pressure at the diffuser outlet is higher than the impeller inlet due to irreversibility. The compression work done by the impeller is accompanied by an increase in temperature, thus, the stagnation temperature at the impeller outlet is 446K. This temperature remains constant through the diffuser. Static pressure and static temperature gradually increase through the compressor. Thus, its maximum values are reached at the diffuser outlet, these are: 249kPa and 429K. The Mach number corresponding to the absolute velocity is maximum, and less than one, at the impeller outlet.

Table I. Design pointperformance for the compressor

Parameter	Impeller inlet		Impeller outlet		Diffuser inlet		Vaned diffuser outlet	
	1		2I		2D		2	
	Ref. [9]	PW	Ref. [9]	PW	Ref. [9]	PW	Ref. [9]	PW
P ₀ (kPa)	100	100	323	323	319	307	269	287
T ₀ (K)	300	300	445	446	445	446	445	446
P (kPa)	93.6	93.6	167	183	200	191	269	249
T (K)	294	294.4	379	380	390	390	430	429
C (m/s)	106	106.3	366	366	335	337	176	188
M _{abs}	0.31	0.31	0.87	0.94	0.86	0.85	0.42	0.45

The results obtained correlate well with Witkowski et al.[9]. Calculations at impeller inlet, 1, are practically the same as those presented in [9]. Result differences in locations 2I, 2D, 2 are due to the correlations considered in the present work. The highest percent difference, corresponding to the static pressure at the impeller outlet, obtained when compared to [9] was 9.6%. This is most likely due to the difference in the energy loss and slip factor calculations. In the present work, correction factors were used in the energy loss calculations. The slip factor formula used in the present work was different from that used in Witkowski et al. [9]. Furthermore, the coefficient F₀ of the slip factor used was adjusted to obtain an appropriate value.

By varying the mass flow rate (0-0.55 kg/s) and the rotational speed (50,000 rpm - 90,000 rpm), the off-design performance was obtained. Fig. 12 shows the effect of variation of mass flow and rotational speed on the pressure ratio.

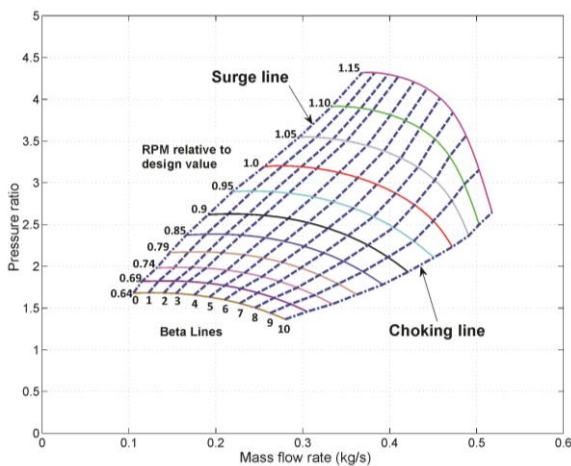


Figure 12. Compressor map: Pressure ratio vs mass flow rate

Solid curve lines shown in Fig. 12 are the rotational speed, these are indicated by dimensionless values that vary from 0.64 (50,000 rpm) to 1.15 (90,000 rpm). These speed lines are obtained by joining pairs of points formed by the pressure ratio and the mass flow rate. The ends of each speed line coincide with the minimum and maximum mass flow rate. Joining imaginarily the minimum mass flow of each speed line it is obtained the surge line, this line is nearly at the left of the maximum efficiency line. Surging is associated with a sudden drop in delivery pressure, and with violent aerodynamic pulsation which is

transmitted throughout the whole machine. The line joining the maximum mass flow points for each rotational speed is called the choking line, that is, no further increase in mass flow is possible beyond this line.

Figure 13 shows the effect of variation of the rotational speed and the mass flow rate on the isentropic efficiency. Curved lines represent the rotational speed, indicated by dimensionless values. Speed lines values are the same as in Fig. 12. The operating point of maximum efficiency on each speed line is approximately the same. Ideally, the compressor should run on the curve connecting these points.

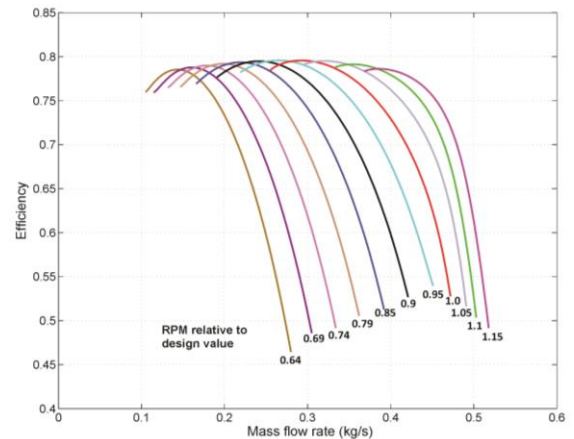


Figure 13. Compressor: Efficiency vs mass flow rate

In Fig. 12, eleven dashed lines intersect the speed lines at a single point, these are called beta lines. Information on mass flow, pressure ratio and efficiency is extracted from each of these points. This information is taken in tabular form, like Tables II, III and IV. These tables may be introduced in a SR-30 turbojet engine model, this procedure is presented in another work. Values of mass flow rate, pressure ratio and isentropic efficiency of the compressor are shown in tables II, III and IV, respectively. The first column of these tables shows the enumeration of beta lines. In the second row of each table, the percentage values of the compressor rotational speeds are shown.

Table II. Tabulated values of the compressor mass flow rate.

β	Rotational speed, N (%)										
	64	69	74	79	85	90	95	100	105	110	115
0	0.11	0.12	0.14	0.16	0.18	0.19	0.21	0.23	0.25	0.26	0.28
1	0.12	0.13	0.15	0.17	0.19	0.21	0.23	0.25	0.27	0.29	0.31
2	0.13	0.15	0.17	0.19	0.21	0.23	0.25	0.27	0.29	0.31	0.33
3	0.15	0.17	0.19	0.21	0.23	0.25	0.28	0.30	0.32	0.34	0.36
4	0.17	0.19	0.21	0.23	0.26	0.28	0.30	0.32	0.35	0.37	0.39
5	0.19	0.21	0.24	0.26	0.28	0.31	0.33	0.35	0.38	0.40	0.42
6	0.22	0.24	0.27	0.29	0.31	0.34	0.36	0.38	0.40	0.43	0.45
7	0.26	0.28	0.30	0.32	0.34	0.36	0.39	0.41	0.43	0.45	0.47
8	0.30	0.32	0.34	0.35	0.37	0.39	0.41	0.43	0.45	0.47	0.49
9	0.33	0.35	0.37	0.38	0.40	0.42	0.44	0.45	0.47	0.49	0.50
10	0.37	0.38	0.40	0.41	0.43	0.44	0.46	0.47	0.49	0.50	0.52

Table III. Tabulated values of the compressor pressure ratio

β	Rotational speed, N (%)										
	64	69	74	79	85	90	95	100	105	110	115
0	1.68	1.68	1.68	1.67	1.66	1.63	1.60	1.56	1.50	1.44	1.37
1	1.81	1.82	1.82	1.81	1.80	1.77	1.73	1.68	1.62	1.55	1.46
2	1.98	1.99	1.99	1.97	1.95	1.92	1.88	1.82	1.74	1.65	1.55
3	2.16	2.17	2.17	2.16	2.14	2.10	2.05	1.98	1.90	1.79	1.66
4	2.37	2.38	2.38	2.37	2.34	2.30	2.24	2.16	2.06	1.93	1.78
5	2.62	2.63	2.62	2.60	2.57	2.52	2.45	2.37	2.25	2.11	1.93
6	2.90	2.90	2.89	2.87	2.83	2.77	2.70	2.60	2.46	2.30	2.09
7	3.21	3.21	3.19	3.17	3.12	3.06	2.98	2.88	2.75	2.57	2.27
8	3.56	3.55	3.53	3.50	3.45	3.39	3.30	3.20	3.07	2.86	2.40
9	3.95	3.94	3.91	3.88	3.83	3.77	3.69	3.59	3.42	3.05	2.51
10	4.38	4.37	4.34	4.30	4.26	4.19	4.11	3.96	3.67	3.19	2.65

Table IV. Tabulated compressor efficiency values.

β	Rotational speed, N (%)										
	64	69	74	79	85	90	95	100	105	110	115
0	75.5	77.7	78.5	78.2	76.9	74.6	71.3	67.0	61.5	54.7	0.46
1	75.4	77.7	78.7	78.6	77.5	75.5	72.5	68.5	63.3	56.7	0.49
2	76.2	78.1	79.0	78.8	77.7	75.7	72.8	68.9	63.8	57.3	0.49
3	76.4	78.3	79.1	79.0	78.1	76.2	73.5	69.8	64.9	58.6	0.51
4	77.9	79.6	79.3	79.2	78.3	76.5	74.0	70.3	65.6	59.4	0.53
5	77.6	79.0	79.5	79.3	78.3	76.7	74.2	70.8	66.3	60.4	0.53
6	78.3	79.3	79.6	79.3	78.3	76.7	74.4	71.2	66.8	61.1	0.53
7	79.0	79.5	79.6	79.2	78.3	76.8	74.8	72.1	68.5	63.5	0.54
8	79.4	79.6	79.5	79.0	78.1	76.9	75.1	72.9	70.0	64.9	0.53
9	79.5	79.5	79.3	79.0	78.2	77.2	75.9	74.0	70.7	63.2	0.51
10	79.3	79.3	79.1	78.8	78.2	77.3	76.1	73.8	70.0	60.2	0.49

Figure 14 compares the results obtained in the present work with those presented by May et al. [12]. The last one, indicated in the legend as paper. Three speed lines of the compression ratio versus mass flow rate graph were compared. The dimensionless values of these rotational speeds are 0.7 (54,000 rpm), 1 (78,000 rpm), and 1.1 (90,000 rpm). Results show a better match as speed increases. In the present work, when the compressor operates near the lowest rotational speed, the choking point is reached with a lower mass flow rate. As speed increases, results of speed lines between the two works match better.

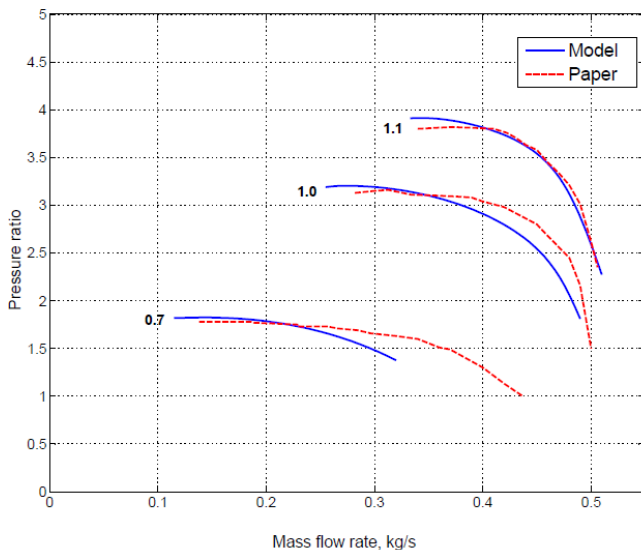


Figure 14. Comparison of results for the compressor map.

B. Turbine Map

Table V shows comparative results between the present work, indicated by PW, and those presented by Witkowski et al. [9], indicated as Ref. [9]. Results are obtained in the design-point performance, that is, at a rotational speed of 78,000 rpm and a mass flow rate of 0.3 kg/s. As shown in the table, static and stagnation pressure decrease across each turbine location. The temperature is highest at the stator inlet. At this location, in the present work, the stagnation temperature is 973K while the static temperature is 967K. The Mach number reaches its maximum value at the stator output, this value is less than 1 (near the transonic region, $M=1$) in both results. If $M=1$, choking will occur. Both results match closely at locations 3 and 4N. It was evidenced that Witkowski et al. [9] has a mistake in the results of static pressure and static temperature, at location

3. A great difference between both results is observed in the absolute and relative velocities, at location 4. This may be due to the tip clearance value used to calculate the tip clearance loss. In the present work a value of 0.54 mm was used, this value was obtained by measurement carried out in the compressor of the experimental module. In Witkowski et al. [9] a value of 2.44 mm was used.

Table V. Design point performance for the turbine

Parameter	Stator inlet		Stator outlet		Rotor outlet	
	Ref. [9]	PW	Ref. [9]	PW	Ref. [9]	PW
P_0 (kPa)	250	250	234	229	120	120
T_0 (K)	973	973	973	973	841	855
P (kPa)	94	244	128	128	115	106
T (K)	294	967	834	841	832	827
C (m/s)	114	114	557	550	141	250
M_{abs}	0.19	0.19	0.98	0.97	0.25	0.37

Off-design performance results are shown in Figures 15 and 16. Figure 15 shows the isentropic efficiency and mass flow rate against the work parameter, $DH/T = (h_4 - h_3)/T_3$. In Fig. 15, each line represents the rotational speed. Colors identify the value of each of these speeds. As the speed increases, the maximum efficiency is reached at a higher value of the working parameter. For each speed, the efficiency remains approximately constant above a certain value of the working parameter. This behavior is due to the fact that the loss coefficients have a small variation in a wide range of incidence. Furthermore, this approximately constant efficiency is greater as the rotational speed increases.

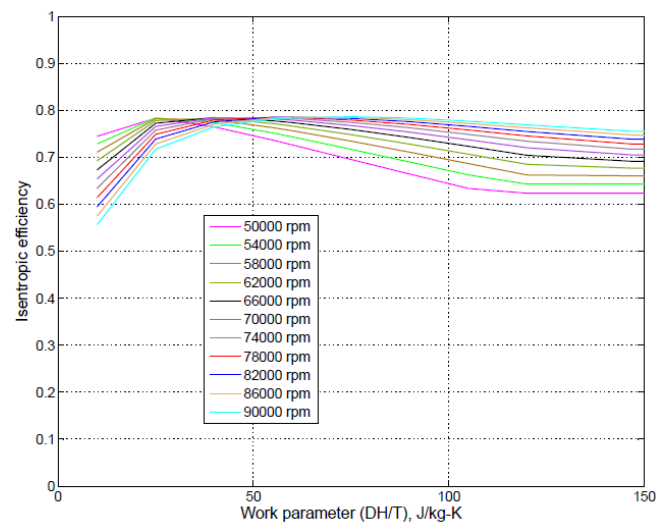


Figure 15. Isentropic efficiency against work parameter.

In Fig. 16 it is observed that for each line of rotational speed, the maximum mass flow increases as the working parameter increases. An increase in mass flow occurs until choking conditions are reached. For all speed lines, choking occurs at the same mass flow rate and at a value of the working parameter greater than 100 J/kg-K.

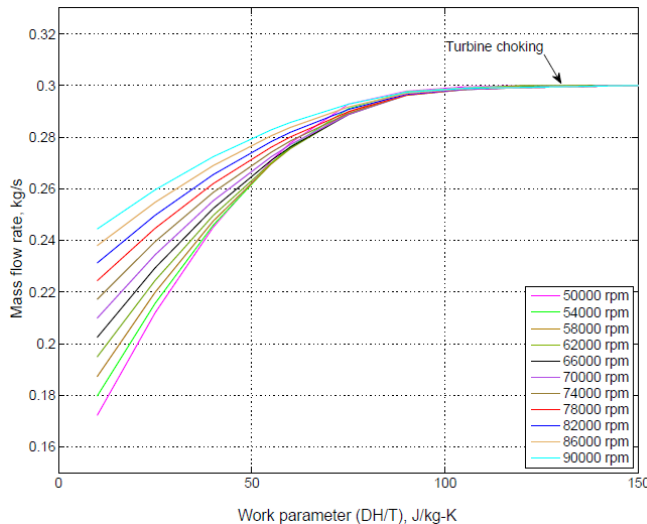


Figure 166. Mass flow rate against workparameter.

In Fig. 17, results of the present work were compared with those presented by May et al. [12], the latter named in the legend as paper. For this comparison, the relationship between mass flow rate and compression ratio was used. In this relationship, graphs of speed lines corresponding to 78,000 rpm are shown. The solid blue line is the one obtained in the present work while the red dashed line is the one obtained in May et al. Graphics are similar only in shape. The difference in the numerical values between both graphs is great. This is due to the fact that the maximum flow taken into account in May et al. [12] is close to 0.22 kg/s, while in this work 0.3 kg/s was considered. The value of 0.3 kg/s is more reasonable, since it represents the combustion mass flow that would be the sum of the air mass flow coming from the compressor plus the fuel mass flow entering the combustion chamber.

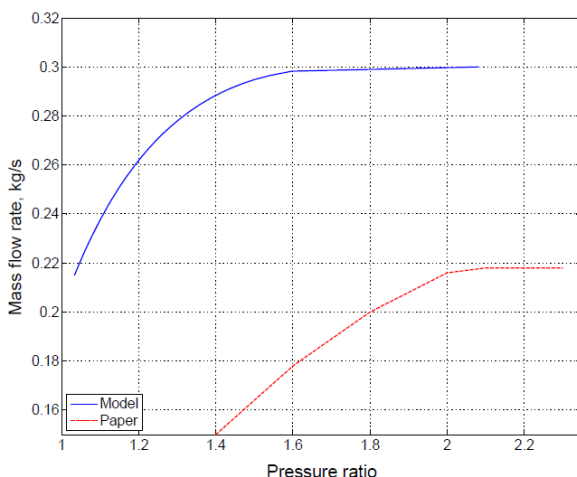


Figure 177. Comparison of results for the turbine map.

Tabulated values of mass flow rate and isentropic efficiency of the turbine are shown in tables VI and VII, respectively. The first column of these tables shows the values of the working parameter (DH/T or simply DHT). The second row of each table shows the percentage values of the rotational speeds of the turbine, these values are the same as for the compressor.

Table VI. Tabulated values of the turbine mass flow rate.

DHT	Rotational speed, N (%)										
	64	69	74	79	85	90	95	100	105	110	115
10	0.17	0.18	0.19	0.19	0.20	0.21	0.22	0.22	0.23	0.24	0.24
25	0.21	0.22	0.22	0.22	0.23	0.23	0.24	0.24	0.25	0.25	0.26
40	0.24	0.25	0.25	0.25	0.25	0.25	0.26	0.26	0.27	0.27	0.27
55	0.27	0.27	0.27	0.27	0.27	0.27	0.27	0.28	0.28	0.28	0.28
70	0.29	0.29	0.29	0.28	0.28	0.28	0.29	0.29	0.29	0.29	0.29
85	0.30	0.30	0.30	0.29	0.29	0.29	0.29	0.29	0.29	0.30	0.30
100	0.30	0.30	0.30	0.30	0.30	0.30	0.30	0.30	0.30	0.30	0.30
115	0.30	0.30	0.30	0.30	0.30	0.30	0.30	0.30	0.30	0.30	0.30
130	0.30	0.30	0.30	0.30	0.30	0.30	0.30	0.30	0.30	0.30	0.30
140	0.30	0.30	0.30	0.30	0.30	0.30	0.30	0.30	0.30	0.30	0.30
150	0.30	0.30	0.30	0.30	0.30	0.30	0.30	0.30	0.30	0.30	0.30

Table VII. Tabulated values of the turbine efficiency.

DHT	Rotational speed, N (%)										
	64	69	74	79	85	90	95	100	105	110	115
10	74.4	72.8	71.1	69.2	67.3	65.4	63.4	61.4	59.5	57.5	0.56
25	78.3	78.4	78.2	77.8	77.2	75.8	75.7	74.8	73.9	72.8	0.72
40	76.5	77.4	78.0	78.3	78.4	78.2	78.2	78.0	77.5	77.0	0.76
55	73.6	75.2	76.3	77.2	77.8	78.4	78.4	78.5	78.5	78.4	0.78
70	70.6	72.6	74.2	75.4	76.4	77.7	77.7	78.1	78.4	78.6	0.79
85	67.5	69.9	71.9	73.5	74.8	76.7	76.7	77.3	77.8	78.2	0.78
100	64.4	67.2	69.4	71.4	73.0	75.4	75.3	76.2	76.9	77.5	0.78
115	62.3	64.4	67.0	69.2	71.1	74.0	74.0	75.0	75.8	76.6	0.77
130	62.3	64.3	66.1	67.7	69.2	72.4	72.4	73.7	74.7	75.6	0.76
140	62.3	64.3	66.1	67.7	69.2	71.7	71.7	72.8	74.0	75.0	0.76
150	62.3	64.3	66.1	67.7	69.2	71.7	71.7	72.8	73.8	74.7	0.75

IV. CONCLUSION

In this work, a one-dimensional analytical model of the compressor and turbine maps was made. The unified slip factor formula recommended by von Backström [13] was used. This formula was used in obtaining the whirl component of the absolute flow velocity at the outlet of the compressor impeller. In the compressor map calculations, the internal and parasitic loss correlations selected by Oh et al. [22] were used. In both maps calculations, iteration loops were used to find the axial component of the absolute flow velocity. Many equations were obtained from the Mollier diagram of the corresponding component. Finally, tabulated forms of the compressor and turbine maps were obtained. The results of the design point calculations for each component were compared with that presented by Witkowski et al. [9], a significant match was observed. Off-design performance results were compared with those obtained by May et al. [12]. These match well in the case of the compressor, turbine results showed similar behavior with a significant numerical values differing. This is most likely due to the fact that May et al. [12] used a maximum flow rate of 0.22 kg/s while the calculation performed used a value of 0.3 kg/s. This value represents the combustion mass flow which would be the sum of both the air mass flow and the fuel mass flow entering the combustion chamber.

In order to further improve the modeling of the component maps, the validation should be developed by using experimental data or with maps obtained from manufacturers. In addition as built construction details should be used when ever available.

ACKNOWLEDGEMENTS:

The authors would like to acknowledge the interest and encouragement of Dr. Allan Valponi. Views express in this paper are those of the authors, and neither of persons acknowledge herein nor of any funding source nor of their institutions.

REFERENCES

- [1] J. Kurzke, "How to get component maps for aircraft gas turbine performance calculations," Proceedings of the ASME 1996 International Gas Turbine and Aeroengine Congress and Exhibition. ASME. doi.org/10.1115/96-GT-164.
- [2] J. Kurzke, Preparing Compressor Maps for Gas Turbine Performance Modeling Manual to Smooth C 8.3, Germany, 2013.
- [3] J. Kurzke, Preparing Turbine Maps for Gas Turbine Performance Modeling Manual to Smooth T 8.2, Germany, 2009.
- [4] A. Lazzaretto, and A. Toffolo, "Analytical and neural network models for gas turbine design and off-design simulation," International Journal of Thermodynamics, vol. 4, issue 4, pp. 173-182, 2001.
- [5] S. Gustafson, and G. Little, "Correlation of transient and steady-state compressor performance using neural networks," Conference Record AUTOTESTCON '92: The IEEE Systems Readiness Technology Conference, Dayton, OH, USA, pp. 69-72, 1992. doi:10.1109/AUTEST.1992.270131.
- [6] Y. Yu, L. Chen, F. Sun, and C. Wu, "Neural-network based analysis and prediction of a compressors characteristic performance map," Applied Energy, vol. 84, issue 4, pp. 48-55, January 2007.
- [7] K. Ghorbanian, and M. Gholamrezaei, "An artificial neural network approach to compressor performance prediction," Applied Energy, vol. 86, issues 7-8, pp. 1210-1221, 2009, ISSN 0306-2619.
- [8] W. Jiang, J. Khan, and R. Dougal, "Dynamic centrifugal compressor model for system simulation," vol. 158, issue 2, pp. 1333-1343, August 2006.
- [9] T. Witkowski, S. White, C. Ortiz, P. Strykowski, and T. Simon, "An artificial neural network approach to compressor performance prediction," Proceedings of the 2003 American Society for Engineering Education Annual Conference and Exposition, December 2003.
- [10] O. Léonard, J. Thomas, and S. Borguet, "Ten years of experience with a small jet engine as a support for education," Journal of Engineering for Gas Turbines and Power-transactions of The ASME - J ENG GAS TURB POWER-T ASME, vol. 131, issue 1, pp. 1-10, January 2009. doi:10.1115/1.2967487.
- [11] H. Oh, E. Yoon, and M. Chung, "An optimum set of loss models for performance prediction of centrifugal compressors," Proceedings of The Institution of Mechanical Engineers Part A-journal of Power and Energy- PROC INST MECH ENG A-J POWER, vol. 211, issue 4, pp. 331-338, 1997. doi:10.1243/0957650971537231.
- [12] D. May, S. Farber, V. Poirier, C. Y. Chen, and I. Stiharu, "Design of a comprehensive condition monitoring system for gas turbine engines," Proceedings of the Canadian Engineering Education Association, August 2011. doi:10.24908/pceea.v0i0.3999.
- [13] T. von Backström, "A unified correlation for slip factor in centrifugal impellers," Journal of Turbomachinery-transactions of The ASME - J TURBOMACH-T ASME, vol. 128, issue 1, January 2006, doi: 10.1115/1.2101853.
- [14] A. Busemann, "Das förderhöhenverhältnis radialer kreiselpumpen mit logarithmisch-spiraligen schaufeln," Math. Mech., vol. 8, pp. 372-384, 1928. doi.org/10.1002/zamm.19280080504.
- [15] A. Stodola, Steam and Gas Turbines: With a Supplement on The Prospects of the Thermal Prime Mover, translated by L.C. Loewenstein, 6th ed. McGraw-Hill, 1927.
- [16] J.D. Stanitz, "Some theoretical aerodynamic investigations of impellers in radial- and mixed-flow centrifugal compressors," Cleveland, Ohio, Transactions of the ASME, vol. 74, pp. 473-476, 1952.
- [17] B. Eck, Fans; Design and Operation of Centrifugal, Axial-Flow, and Cross-Flow Fans, Pergamon, 1972. ISBN 10:0080158722.
- [18] S.L. Dixon, and C.A. Hall, Fluid Mechanics and Thermodynamics of Turbomachinery, Butterworth-Heinemann, 7th ed., 2014. ISBN 13:978-0-12-415954-9.
- [19] P. Walsh, and P. Fletcher, Gas Turbine Performance, Wiley-Blackwell, United States, 2nd ed., March 2004. ISBN: 978-0-632-06434-2.
- [20] H.I.H. Saravanamuttoo, G.F.C. Rogers, P. Straznicky, H. Cohen, and A.C. Nix, Gas Turbine Theory, Pearson Education Limited, United Kingdom, 7th ed., 2017. ISBN: 9781-292-09313-0.
- [21] F.J. Wiesner, "A review of slip factors for centrifugal impellers," Journal of Engineering for Gas Turbines and Power, vol. 89, issue 4, pp. 558-566, October 2011. doi:10.1115/1.3616734.
- [22] H. Oh, E. Yoon, and M. Chung, "An optimum set of loss models for performance prediction of centrifugal compressors," Proceeding of the Institution of Mechanical Engineers Part A-journal of Power and Energy - PROC INST MECH ENG A-J POWER, vol. 211, issue 4, pp. 331-338, June 1997. doi: 10.1243/0957650971537231.
- [23] M.P. Boyce, Gas Turbine Engineering Handbook, Elsevier Butterworth-Heinemann, Waltham, MA, USA, 4th ed., 993 pages, 2012. ISBN 13: 9780123838421.